Active tectonics of the Beichuan and Pengguan faults at the eastern margin of the Tibetan Plateau

Alexander L. Densmore,[1] Michael A. Ellis,[2] Yong Li,[3] Rongjun Zhou,[4] Gregory S. Hancock,[5] and Nicholas Richardson[6]

Received 28 April 2006; revised 27 February 2007; accepted 2 April 2007; published 17 July 2007.

[1] The steep, high-relief eastern margin of the Tibetan Plateau has undergone rapid Cenozoic cooling and denudation yet shows little evidence for large-magnitude shortening or accommodation generation in the foreland basin. We address this paradox by using a variety of geomorphic observations to place constraints on the kinematics and slip rates of several large faults that parallel the plateau margin. The Beichuan and Pengguan faults are active, dominantly dextral-slip structures that can be traced continuously for up to 200 km along the plateau margin. Both faults offset fluvial fill terraces that yield inheritance-corrected, cosmogenic ^{10}Be exposure ages of <15 kyr, indicating latest Pleistocene activity. The Pengguan fault appears to have been active in the Holocene at two sites along strike. Latest Quaternary apparent throw rates on both faults are variable along strike but are typically <1 mm yr^{-1}. Rates of strike-slip displacement are likely to be several times higher, probably ~1–10 mm yr^{-1} but remain poorly constrained. Late Quaternary folding and dextral strike-slip has also occurred along the western margin of the Sichuan Basin, particularly associated with the present-day mountain front. These observations support models for the formation and maintenance of the eastern plateau margin that do not involve major upper crustal shortening. They also suggest that activity on the margin-parallel faults in eastern Tibet may represent a significant seismic hazard to the densely populated Sichuan Basin. **Citation:** Densmore, A. L., M. A. Ellis, Y. Li, R. Zhou, G. S. Hancock, and N. Richardson (2007), Active tectonics of the Beichuan and Pengguan faults at the eastern margin of the Tibetan Plateau, *Tectonics*, *26*, TC4005, doi:10.1029/2006TC001987.

1. Introduction

[2] The Longmen Shan region at the eastern margin of the Tibetan Plateau, adjacent to the Sichuan Basin (Figure 1), is characterized by elevations of up to 7500 m above sea level and by topographic relief of more than 5 km over distances of less than 50 km. The plateau margin has the steepest topographic gradient of any edge of the modern-day plateau. It is deeply incised by tributaries to the Yangzi River, with local fluvial (valley floor to ridge crest) relief in excess of 3 km and steep bedrock river channels [*Kirby et al.*, 2003]. Thermal histories derived from a variety of thermochronometers show rapid cooling rates during the late Cenozoic and up to 7–10 km of denudation along a narrow zone within the plateau margin, beginning either ~20 Ma [*Arne et al.*, 1997] or 9–13 Ma [*Kirby et al.*, 2002; *Clark et al.*, 2005].

[3] The origins of this extreme relief and rapid late Cenozoic denudation, and the role of upper crustal faults in the evolution of the plateau margin, have been a matter of debate [*Chen et al.*, 1994; *Kirby et al.*, 2000, 2002, 2003; *Clark et al.*, 2005; *Richardson et al.*, 2007]. A network of steeply dipping, generally northeast-trending faults have been mapped along the margin [*Chen et al.*, 1994; *Burchfiel et al.*, 1995] (Figure 1). These faults accommodated significant crustal shortening during the Late Triassic Indosinian Orogeny [*Chen and Wilson*, 1996; *Li et al.*, 2003], which has led to the identification of the Longmen Shan region as a major thrust zone that was reactivated in the India-Asia collision [e.g., *Avouac and Tapponnier*, 1993; *Xu and Kamp*, 2000]. Folding and minor faulting of Cenozoic age have been described in the westernmost Sichuan Basin [*Burchfiel et al.*, 1995]. Geological evidence for widespread Quaternary thrusting, however, is sparse and equivocal [*Chen et al.*, 1994; *Burchfiel et al.*, 1995], and Global Positioning System (GPS) surveys constrain active shortening across the entire Longmen Shan to 4.0 ± 2.0 mm y^{-1} relative to the Sichuan Basin [*Zhang et al.*, 2004]. Cenozoic sediment is thin and discontinuous in the Sichuan Basin (Figure 2), with a maximum thickness of only about 500 m of Quaternary sediment adjacent to the Longmen Shan mountain front [*Chengdu Hydrological and Engineering Team*, 1979, 1985].

[4] The combination of high relief, low present shortening rates, and negligible Cenozoic accommodation gener-

[1] Institute of Hazard and Risk Research and Department of Geography, Durham University, Durham, UK.
[2] Center for Earthquake Research and Information, University of Memphis, Memphis, Tennessee, USA.
[3] National Key Laboratory of Oil and Gas Reservoir Geology and Exploitation, Chengdu University of Technology, Chengdu, Sichuan, China.
[4] Seismological Bureau of Sichuan Province, Chengdu, Sichuan, China.
[5] Department of Geology, College of William and Mary, Williamsburg, Virginia, USA.
[6] Department of Earth Sciences, Swiss Federal Institute of Technology, Zurich, Switzerland.

0278-7407/07/2006TC001987$12.00

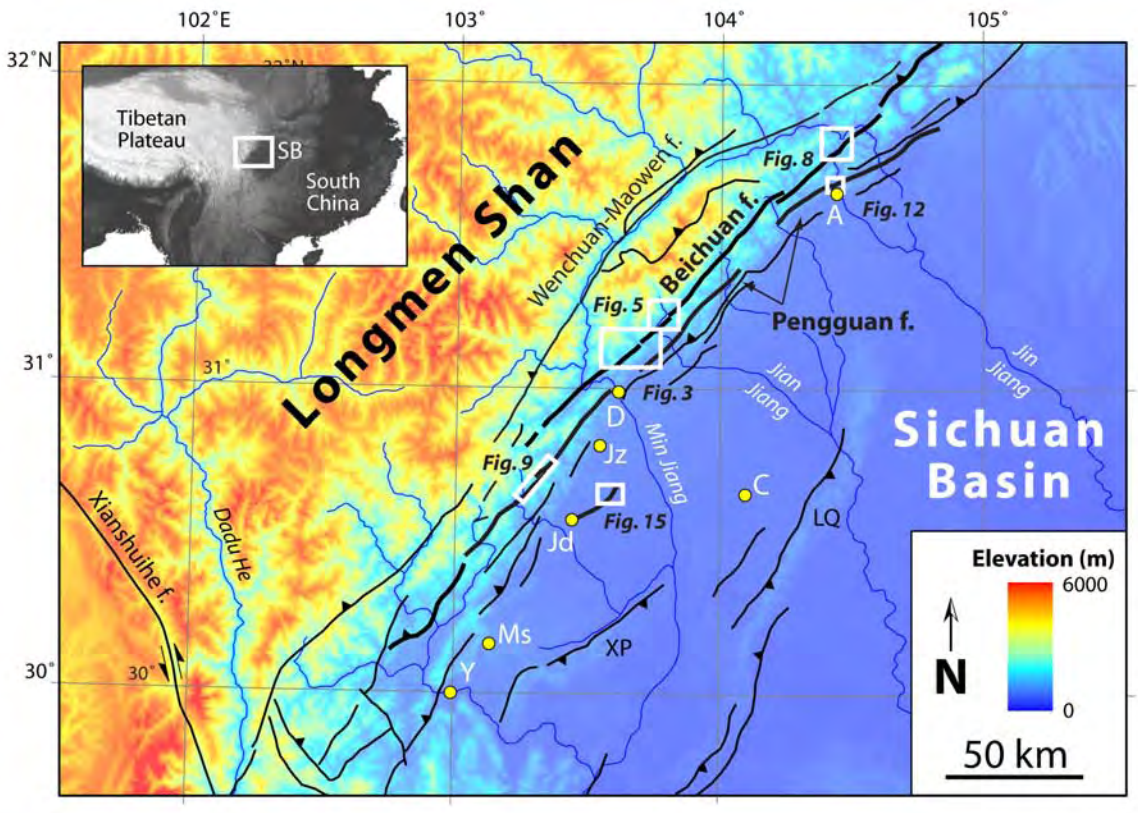

Figure 1. Location map of Longmen Shan and western Sichuan Basin. Topography is taken from SRTM data with 3 arcsec resolution. Major river systems are shown in blue. Faults (black lines) are simplified from the work of *Burchfiel et al.* [1995] and our mapping. Black boxes show locations of subsequent figures. Major cities: A, An Xian; C, Chengdu; D, Dujiangyan; Y, Yaan. Locations described in text: Jd, Jindong; Jz, Jiezi; Ms, Mingshan. Anticlines in the western Sichuan Basin: LQ, Longquan; XP, Xiong Po. Inset shows location of study area (box) and Sichuan Basin (SB) relative to Tibetan Plateau.

ation inspired *Royden et al.* [1997] to invoke lateral expulsion of fluid lower crust from beneath eastern Tibet into the Longmen Shan region. This model of orogenesis, which has been elaborated by *Clark and Royden* [2000] and *Clark et al.* [2006], implies primarily vertical movement of the plateau margin due to impedance of lateral flow by the thick, cold Yangzi Craton that underlies the Sichuan Basin [*Lebedev and Nolet*, 2003]. While the model provides compelling explanations of many of the topographic features of the Longmen Shan region [*Clark et al.*, 2006], it is not clear how such large-scale late Cenozoic rock uplift has affected the network of faults along the margin nor is it clear whether these margin-parallel faults may have also accommodated northeast-directed dextral simple shear during the India-Asia collision, as proposed by *England and Molnar* [1990]. The northwest-trending Xianshuihe and Ganzi faults, southeast of the Longmen Shan, have accommodated ~60 and ~100 km of sinistral displacement, respectively, since at least 2–4 Ma [*Wang et al.*, 1998; *Wang and Burchfiel*, 2000]. It is not known whether comparable dextral movement has occurred on the margin-parallel faults.

[5] We suggest that a necessary step in understanding the evolution of the eastern Tibetan Plateau is to document the late Cenozoic activity and kinematics of the major faults along the plateau margin. With the exception of work by *Chen et al.* [1994] and *Burchfiel et al.* [1995], and a more detailed study of the Min Jiang fault by *Kirby et al.* [2000], this has not yet been done. In this reconnaissance study, we address this shortcoming by presenting geomorphic evidence for late Cenozoic slip along several of the faults in the Longmen Shan and western Sichuan Basin. We use a combination of techniques, including field mapping, image interpretation, surveying of offset geomorphic markers, trenching, and cosmogenic radionuclide dating. These methods allow us to examine the history of fault slip on timescales of 10^3–10^4 yr, bridging the gap between the geological and geodetic approaches that have been previously applied in the region.

2. Geological History of the Eastern Plateau Margin

[6] The present-day Longmen Shan region is roughly coincident with the position of a Mesozoic collisional plate margin that developed during the closure of Paleo-Tethys

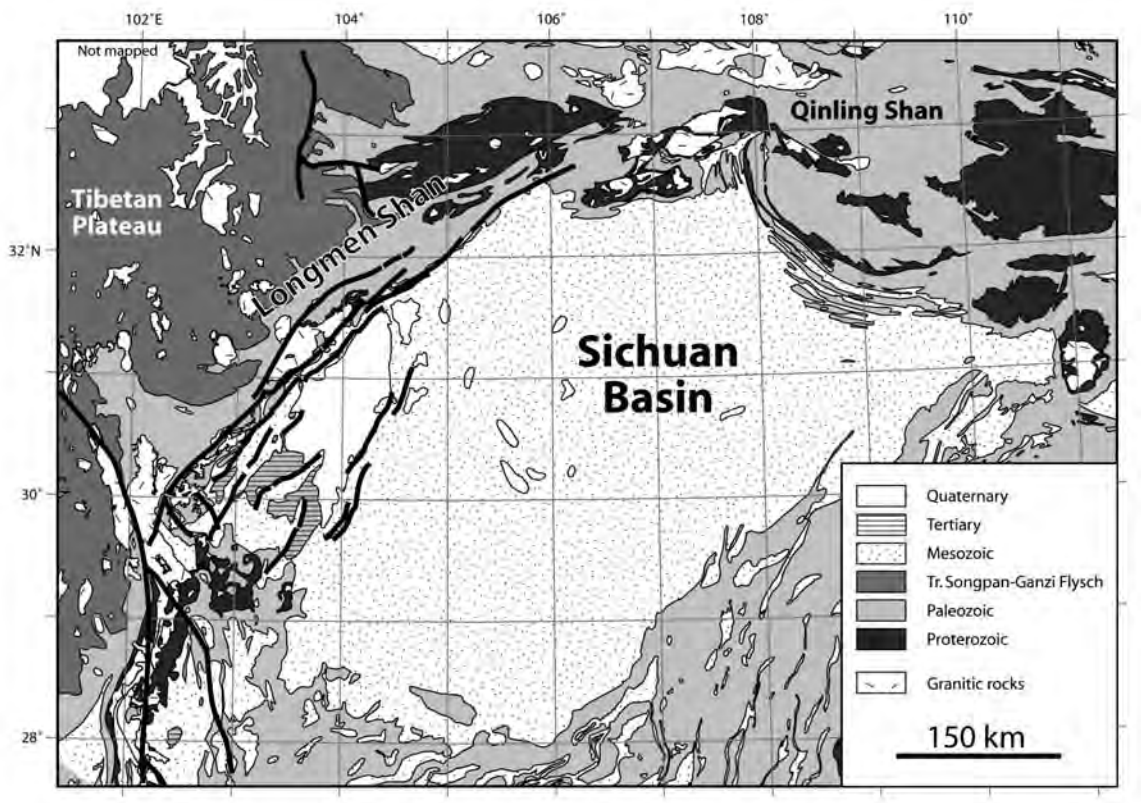

Figure 2. Simplified geological map of the Sichuan Basin and surrounding areas, modified from the work of *Ma* [2002]. Heavy black lines show the major active faults in the Longmen Shan and western Sichuan Basin, modified from the work of *Ma* [2002], *Burchfiel et al.* [1995], and our mapping. Note that Tertiary and Quaternary rocks are limited to the westernmost Sichuan Basin, adjacent to the Longmen Shan.

and the collision of the Qiangtang block with the North China-Kunlun-Qaidam and South China blocks [*Yin and Nie*, 1996; *Zhou and Graham*, 1996; *Li et al.*, 2003; *Weislogel et al.*, 2006]. Deformation began in the Late Triassic Indosinian Orogeny [*Li et al.*, 2003] and continued through to the Late Cretaceous. During the collision, a complex package of rocks, including Triassic marine sedimentary rocks of the Songpan-Ganzi remnant ocean basin (Figure 2) [*Zhou and Graham*, 1996], was thrust to the southeast over the margin of the South China block, creating a Late Triassic foreland basin [*Burchfiel et al.*, 1995; *Chen and Wilson*, 1996; *Li et al.*, 2003]. Shortening was initially accommodated largely on the Wenchuan-Maowen and Beichuan faults but later migrated southeastward onto the Pengguan fault (Figure 1) [*Chen et al.*, 1995; *Chen and Wilson*, 1996; *Li et al.*, 2003]. Thus, most of the major margin-parallel faults visible in Figure 1 have existed since at least Late Triassic time [*Burchfiel et al.*, 1995; *Chen and Wilson*, 1996; *Li et al.*, 2003].

[7] In the Sichuan Basin, deposition of continental clastic sediment derived from the collision continued through the Mesozoic and into early Cenozoic time [*Ma*, 2002]. These sediments are now capped by a widespread erosional unconformity that extends over much of the Sichuan Basin (Figure 2) [*Burchfiel et al.*, 1995; *Richardson et al.*, 2007]. Overlying this unconformity is a poorly consolidated, generally clast-supported cobble to boulder conglomerate, up to several hundred meters thick, that is exposed along the present-day mountain front at the western basin margin. The conglomerate contains granitic, metamorphic, volcanic, and sandstone clasts and is collectively known to Chinese geologists as the Dayi Formation [*Burchfiel et al.*, 1995]. It is commonly interpreted as debris-flow fan sediments that record the initial erosion of metamorphic and igneous basement in the Longmen Shan to the west. While this represents an important time marker in the Longmen Shan region, the age of the Dayi Formation is unfortunately very poorly constrained. Similar rocks exposed to the south of the Longmen Shan region have been assigned depositional ages of 4.2–2.6 Ma on the basis of magnetostratigraphy [*Ji et al.*, 1997; *Jiang and Wu*, 1999], although other authors have suggested Quaternary ages [*Deng et al.*, 1994]. *Burchfiel et al.* [1995] considered the Dayi Formation and related rocks to be of probable Neogene age. Undisputed Quaternary deposits, which appear to be mineralogically distinct from the Dayi Formation [*Richardson et al.*, 2005], are limited to the westernmost Sichuan Basin and consist of thin (<500 m; *Chengdu Hydrological and Engineering*

Team [1979, 1985]), low-gradient alluvial fans that radiate from the major drainage basin outlets.

3. Methods and Techniques

[8] There is some disagreement among different investigators about the locations, names, kinematics, and activity on the major margin-parallel faults in the Longmen Shan region [e.g., *Chen et al.*, 1994; *Burchfiel et al.*, 1995; *Chen and Wilson*, 1996; *Xu and Kamp*, 2000]. In this paper, we attempt to synthesize these studies with our own field observations at a number of sites in the Longmen Shan region. Because of the scale of the region, the high local relief (commonly in excess of 3500 m), dense vegetation, regionally poor exposure, and locally dense settlement and agriculture, this study is necessarily reconnaissance in nature. Rather than presenting exhaustive mapping of each structure, we focus here on several key field areas where each fault can be observed and constrained.

[9] The fault names that we adopt, and the locations of detailed site analyses, are shown in Figure 1. From west to east, the primary margin-parallel structures are (1) the Wenchuan-Maowen fault, (2) the Beichuan fault, (3) the Pengguan fault, and (4) faults and folds in the westernmost Sichuan Basin, including the Dayi fault. We focus here on the margin-parallel structures that show the most abundant evidence for Quaternary displacement. While evidence for active dextral slip on the Wenchuan-Maowen fault (Figure 1) between Wenchuan and Maowen was noted by *Burchfiel et al.* [1995], we were unable to find unequivocal signs of datable, Quaternary displacement, and we do not discuss it further.

3.1. Fault Mapping

[10] We mapped the active traces of the Beichuan, Pengguan, and Dayi faults using a combination of Landsat 7 panchromatic and ASTER satellite imagery and Chinese aerial photographs. These preliminary maps were used to guide focused field observations at specific sites where geomorphic indicators of Quaternary activity might be preserved. In the field, we looked for standard landforms associated with active faults: scarps or offset surfaces in Quaternary deposits, offset stream channels, shutter ridges, linear valleys, and benches or beveled hillslopes. Where appropriate, offset landforms were surveyed using either an electronic total station or a handheld laser surveying device (Laser Atlanta Advantage) and reflector, with a measurement repeatability of better than ±10 cm. Positions were determined using handheld GPS receivers, and elevations were taken from GPS measurements or from Chinese topographic maps (scales of 1:25000 or 1:50000). Positions of field locations are given in Universal Transverse Mercator (UTM) coordinates (zone 48, WGS84 datum).

[11] It is important to note that unequivocal slip sense indicators are very difficult to find in the region because of poor exposure of the faults. In addition, the steep terrain means that strike-slip displacement may lead to apparent local dip-slip offsets. With this in mind, we discuss our observations below in terms of apparent vertical (throw) offset and rates. We regard consistent dip-slip separation across a fault over scales of at least several to several tens of kilometers as compelling evidence for a dip-slip component of motion. In contrast, variable senses of separation on shorter length scales are likely to be localized responses to changes in topography or fault strike.

[12] While we use the names of the Beichuan and Pengguan faults to refer to presently active structures in the Longmen Shan, it is worth pointing out that these faults formed during the Late Triassic Indosinian Orogeny [*Burchfiel et al.*, 1995; *Chen and Wilson*, 1996; *Li et al.*, 2003] and that the presently active faults are largely, but not wholly, coincident with the surface traces of the older structures.

3.2. Trenching

[13] To establish the timing of the most recent slip on the Pengguan fault, we excavated a 1.5-m-deep trench across the fault at Qinshiping (331848/3391429). Because we did not find suitable piercing lines across the fault, our analysis of the trench was limited to the trench wall. One wall of the trench was cleaned and logged at a scale of 1:10 following standard procedures [e.g., *McCalpin*, 1996]. Age constraints on the units exposed in the trench face were provided by ^{14}C analysis of charcoal fragments. We also partially reexcavated a trench across the Beichuan fault near Baishuihe (386572/3459531) that was originally dug and interpreted by *Zhou et al.* [2007]. We collected several additional samples for ^{14}C analysis from one wall of this trench.

3.3. Dating of Depositional Surfaces Using Cosmogenic Radionuclides

[14] Most of the geomorphic indicators of fault slip in the Longmen Shan region involve deformation of depositional surfaces or landforms, such as fluvial fill terraces or sediment fans. In the absence of well-exposed stratigraphy or abundant organic material, dating such landforms is notoriously difficult. For this reason, we determined landform ages by measuring the concentration of in situ cosmogenic ^{10}Be in quartz extracted from fluvial deposits in several locations. Samples consisted of either (1) amalgamated depth profiles of several dozen granitic cobbles collected from the deposit surface and from various depths within the deposit, or (2) in one case, a sample collected from the top of a large (2.5 m) boulder buried within a sediment fan. For the amalgamated samples, several dozen fluvially transported granitic cobbles, with diameters of 4–8 cm, were collected at several depths (±0.1 m) between 0.3 and 3.5 m below the terrace surface by sampling exposures created by recent construction within the deposits. We selected cobbles only from visibly stratified layers of obvious fluvial origin below the cultivated surface layer. Each cobble was crushed individually, and equal aliquots were amalgamated into a single subsample from each depth, yielding an average ^{10}Be concentration for that depth [*Anderson et al.*, 1996]. Quartz was isolated from all samples following a modification of the technique of *Kohl and Nishiizumi* [1992]. Isolation of ^{10}Be from quartz and measurement of $^{10}Be/^{9}Be$ ratios by accelerator mass

Table 1. Cosmogenic Radionuclide Samples and Analytical Results

Sample	Sample Type	Number of Cobbles	Lat	Elev, m	Latitude/Altitude Correction Factor[a]	Horizon Correction Factor	Sample Depth, m	[^{10}Be] 10^5 atoms/g	^{10}Be Model Age, kyr[b]	Inheritance Corrected Age, kyr[c]
DLS-1A	Profile	24	31.2821°N	1205	2.12	0.977	0.50–0.70	0.85 ± 0.09	13.1 ± 2.5	12.2 ± 3.9
DLS-1B		27	31.2821°	1205	2.12	0.977	1.40–1.60	0.43 ± 0.07	14.1 ± 3.2	
XH-1A	Profile	16	31.6752°	601	1.37	0.974	0.25–0.35	0.45 ± 0.07	8.29 ± 2.0	4.2 ± 2.1
XH-1B		17	31.6752°	601	1.37	0.974	1.60–1.80	0.31 ± 0.09	18.8 ± 6.4	
XH-1C		22	31.6752°	601	1.37	0.974	2.90–3.10	0.24 ± 0.06	43.1 ± 15	
GY-1	Surface	34	31.1343°	1104	1.97	0.974	0.00–0.80	0.31 ± 0.05	4.22 ± 1.0	NA
GY-2	Boulder	NA	31.1343°	1104	1.97	0.974	0.00-0.05	0.80 ± 0.08	8.26 ± 1.5	NA

[a]Correction factors calculated following the work of *Stone* [2000].
[b]Assumes sea level, high-latitude ^{10}Be production rate of 5.10 a g^{-1} yr^{-1} [*Stone*, 2000], terrace soil density of 1.5 g cm^{-3}, and rock sample density of 2.7 g cm^{-3}.
[c]Calculated using pairs correction technique in the work of *Anderson et al.* [1996].

spectrometry was completed by PRIME Lab at Purdue University. The sample locations, measured ^{10}Be concentrations, and model ages are given in Table 1. Also given are elevation, latitude, and horizon shielding correction factors used to determine the ^{10}Be production rate, following the method of *Stone* [2000]. Horizon shielding was determined by measuring the compass direction and azimuth angle to all major breaks (for example, peaks and valleys) in the topography surrounding the sample site, filling in straight lines between each measured point, and integrating this simplified topographic profile to determine the fraction of sky shielded by topography.

[15] The ^{10}Be concentrations were translated to landform age using several methods. The age for the amalgamated depth profile with one sample pair (DLS-1; Table 1) was evaluated using the sample pairs technique of *Anderson et al.* [1996] on the upper two samples in each set. This technique corrects for the possible presence of inherited ^{10}Be that may have been acquired during erosion and transport of the cobbles. An inheritance-corrected depositional age, t, is obtained from:

$$t = \frac{1}{\lambda} \ln\left(\frac{\Delta P}{\Delta P - \lambda \Delta N}\right) \quad (1)$$

where ΔP is the difference in production rate between the two sample depths, ΔN is the difference in ^{10}Be concentration, and λ is the decay constant for ^{10}Be. We use a modification of this inheritance-correction technique for evaluating the results of XH-1 (Table 1), where three amalgamated subsamples from different depths are available. Given that the ages obtained on these samples are much less than the half-life of ^{10}Be, we can safely ignore decay. *Hancock et al.* [1999] related deposit age (t), depth (z), initial inherited ^{10}Be concentration (N_{in}), and final concentration ($N[z, t]$) in the absence of decay with the following equation:

$$N(z,t) = P_0 t \exp\left(-\frac{z}{z*}\right) + N_{in} \quad (2)$$

where P_0 is the production rate at the surface and $z*$ is a decay length scale given by Λ/ρ, where ρ is the density of the overlying material and Λ is the absorption mean free path. We use a value of 150 g cm^{-2} for Λ [*Brown et al.*, 1992]. We use equation (2) to obtain an estimate for both t and N_{in} through linear regression of the relationship between $\exp(-z/z*)$ and $N(z, t)$, both of which are known for each sample depth (Table 1).

[16] For the surface samples GY-1 and GY-2 (Table 1), ages were calculated assuming a constant production rate over the period of exposure. These samples likely have some component of inherited ^{10}Be, but this cannot be evaluated given the results obtained. The ages shown for these samples in Table 1 should therefore be considered maximum ages.

4. Results

4.1. Beichuan Fault

[17] The Beichuan fault (also referred to as the Yingxiu-Beichuan fault) formed one of the major active thrusts during the Late Triassic Indosinian Orogeny [*Chen and Wilson*, 1996; *Li et al.*, 2003]. *Chen and Wilson* [1996] argued that the Beichuan fault thrusts Mesoproterozoic basement and metamorphosed Paleozoic rocks toward the southeast over generally unmetamorphosed rocks of the frontal Longmen Shan. *Burchfiel et al.* [1995] showed that the Beichuan fault both bounds and cuts the southern margin of the Pengguan basement massif (Figure 2). They mapped the present-day Beichuan fault as a steeply northwest-dipping structure that has accommodated late Cenozoic transpressive displacement through a combination of thrust and minor dextral movement.

[18] On satellite imagery, the Beichuan fault can be continuously traced for approximately 200 km through the Longmen Shan region. Where we have examined it, the active trace of the Beichuan fault appears to be steeply northwest dipping to vertical, and shows abundant evidence for Quaternary dextral strike-slip displacement, with minor and locally variable components of dip slip. Below, we describe detailed observations from four separate sites along the Beichuan fault.

4.1.1. Gaoyuan

[19] North of Dujiangyan, the Beichuan fault forms a linear valley that extends northeast from the Min Jiang

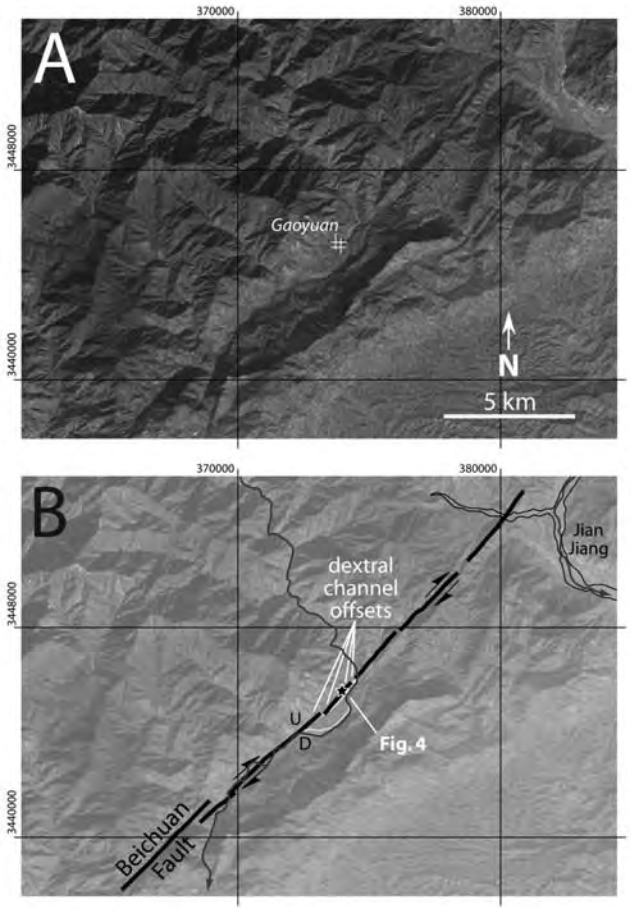

Figure 3. (a) Uninterpreted aerial photograph of the Beichuan fault near Gaoyuan. See Figure 1 for location. In this and subsequent figures, *X*-*Y* coordinates are in UTM projection, zone 48N. (b) Interpreted photograph of the same area. Active fault trace is marked by thick black lines. U and D mark the locally upthrown and downthrown blocks, respectively. Thin white lines show margins of fluvial fill terrace cut by the Beichuan fault. Location of cosmogenic samples GY-1 and GY-2 is shown by black star.

(Jiang is Chinese for river) toward the Jian Jiang (Figure 1). Near the village of Gaoyuan (373630/3445246, Figure 3), the fault trace is marked by a series of benches, shutter ridges, and small (5–40 m) dextral stream channel offsets along the northwestern valley wall. At Gaoyuan, the fault forms a prominent scarp trending 040, NW side up, across a small (~100 m across) sediment fan (Figure 4). Vertical offset of the fan surface is 3.0 ± 0.2 m within a narrow (10 m) fault zone.

[20] We collected two sediment samples from the Gaoyuan fan for ^{10}Be analysis. The first sample (GY-1) consisted of 34 granitic cobbles taken from the fan surface. Because the fan appears to have been cultivated to a depth of approximately 0.8 m, this amalgamated sample should reflect an average ^{10}Be concentration for the uppermost ~1 m of the fan deposit. In addition, a single sample (GY-2) was collected from the top of a large (2.5-m diameter) granitic boulder protruding ~1.2 m above the fan surface. The amalgamated sample GY-1 yielded a ^{10}Be exposure age of 4.2 ± 1.0 kyr, while boulder sample GY-2 yielded a ^{10}Be exposure age of 8.3 ± 1.5 kyr (Table 1). Because the cosmogenic ^{10}Be production rate decays exponentially with depth, and because bioturbation and cultivation have mixed the uppermost 0.8 m of the fan deposit, the age given by GY-1 is an absolute minimum estimate for the age of deposition on the fan surface. In contrast, the large size of the boulder from which sample GY-2 was taken, and its depth of burial within the fan, makes it unlikely that the boulder has rotated or otherwise moved significantly after deposition. Because the GY-2 boulder may have accumulated an unknown concentration of ^{10}Be during transport to its current position, we interpret GY-2 as a maximum estimate of fan surface age. Taken together, the ^{10}Be data imply a minimum apparent throw rate of 0.36 ± 0.07 mm yr^{-1} on the Beichuan fault at this site.

4.1.2. Baishuihe

[21] To the northeast of Gaoyuan, the Beichuan fault is visible as a series of generally southeast-facing scarps, dextral stream offsets, and aligned saddles near the town of Baishuihe (Figure 5). Just north of Baishuihe, the fault forms a southeast-facing, 4.5 ± 1.0 m scarp across an undated fill terrace surface, ~60 m above the modern level of the Jian Jiang (Figure 6a). Several hundred meters to the northeast, a small stream is offset 6.4 ± 0.2 m in a dextral sense (385706/3458591, Figure 6b). The dextral offset coincides with a linear, southeast-facing scarp that is 0.5 ± 0.1 m high and trends 062. The stream is incised into colluvium which drapes the fill terrace surface; therefore, the stream offset is younger than the terrace offset. The stream offset suggests a strike-slip to dip-slip ratio of at least 12:1 on the Beichuan fault at this location; given that strike-slip displacement of a sloping surface can also produce

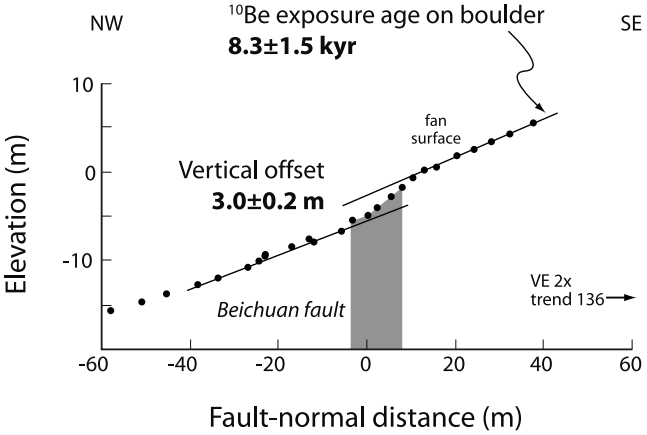

Figure 4. Survey of small alluvial fan cut by the Beichuan fault at Gaoyuan. See Figure 3 for location. The fan surface is offset 3.0 ± 0.2 m across the fault (shown schematically by the grey box). A 2.5-m-diameter granitic boulder on the fan surface yields a ^{10}Be exposure age of 8.3 ± 1.5 kyr (Table 1), implying a minimum apparent throw rate of 0.36 ± 0.07 mm yr^{-1} on the fault.

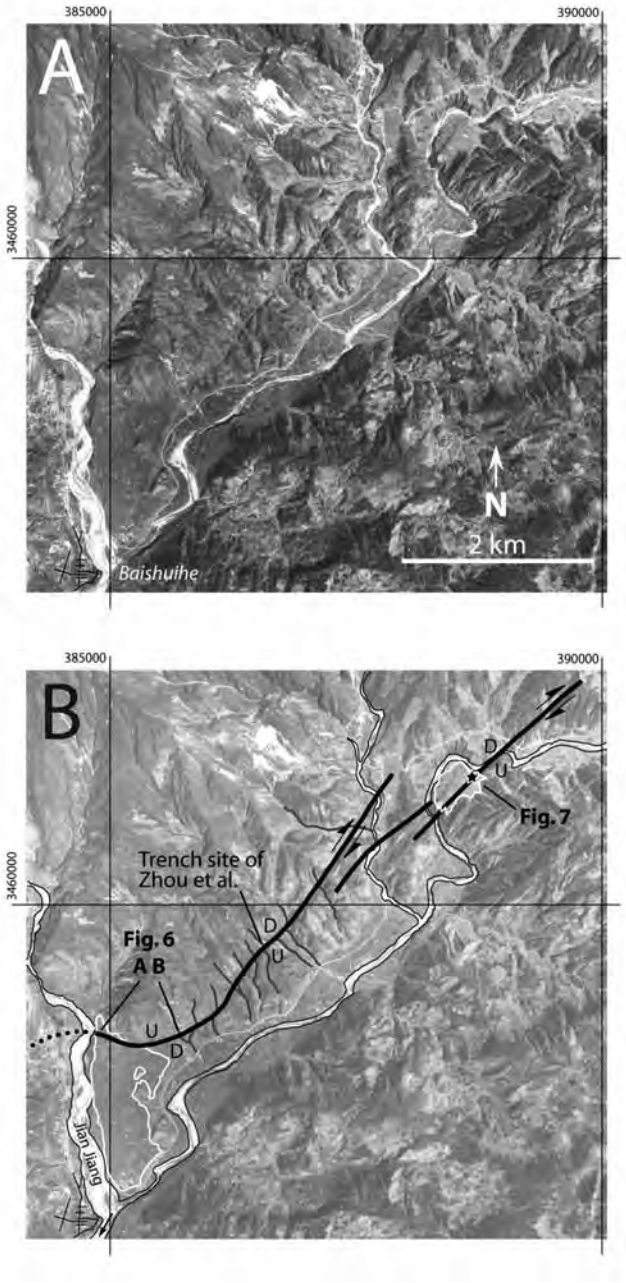

Figure 5. (a) Uninterpreted aerial photograph of the Beichuan fault near Baishuihe (located in lower left corner of image). See Figure 1 for location. (b) Interpreted photograph of the same area. Active fault trace is marked by thick black lines. U and D mark the locally upthrown and downthrown blocks, respectively. Note that sense of separation across the fault changes along strike to the northeast of Baishuihe. Dark grey lines show channels which are laterally offset by the fault. Thin white lines show margins of fluvial fill terraces cut by the fault. Location of cosmogenic sample DLS-1 is shown by black star.

apparent dip-slip offset, we regard this as a minimum ratio. In the absence of age control on the terrace or the overlying colluvium, we are unable to assign a slip rate.

[22] The fault can be followed toward the northeast through several linear valleys and aligned saddles to the trench site in the work of *Zhou et al.* [2007], which sits in a narrow, linear depression trending 038 and bounded to the southeast by a prominent shutter ridge (Figure 5). Note that the sense of apparent vertical separation across the fault here is opposite to that at the locations in Figure 6, ~1500 m to

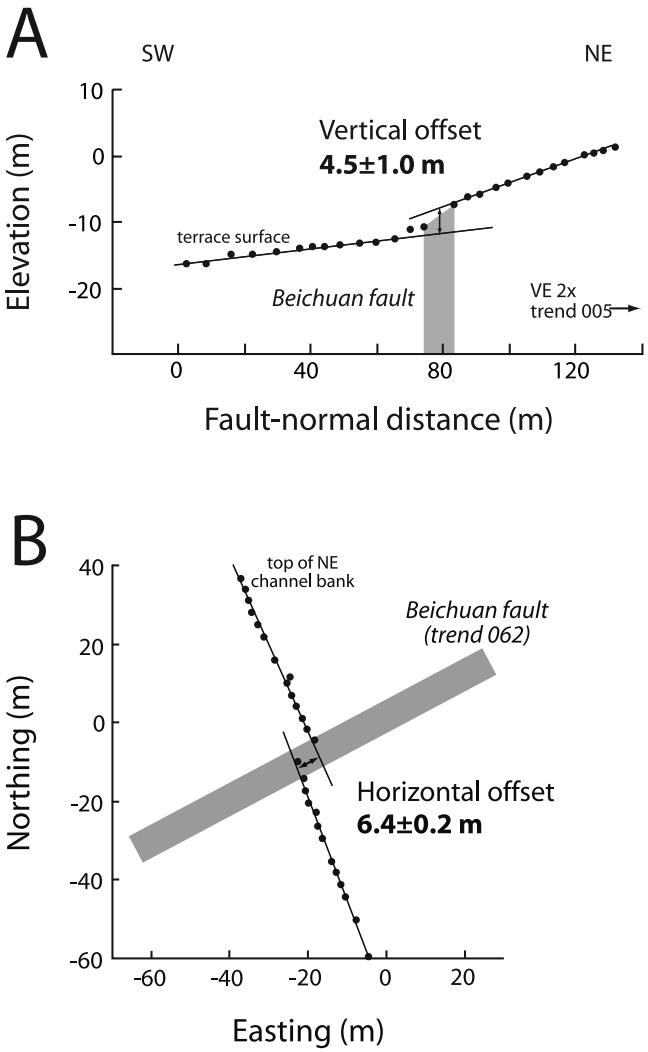

Figure 6. Surveys of geomorphic features offset by the Beichuan fault near Baishuihe. See Figure 5 for locations. (a) Scarp on fluvial fill terrace formed by the Beichuan fault. The surface of this undated terrace is offset 4.5 ± 1.0 m across the fault (shown schematically by the grey box). (b) Map view of small channel offset by the Beichuan fault. Black dots show survey points along the top of the northeastern channel bank, which is dextrally offset 6.4 ± 0.2 m; the thalweg yields a similar offset. The offset corresponds to a 0.5 ± 0.1 m scarp (NW side up) along the fault trace.

Table 2. Radiocarbon Samples and Analytical Results[a]

Sample	Material	$^{13}C/^{12}C$ Ratio, per mil	Conventional Radiocarbon Age, y BP
030203-4	Charcoal	−27.6	930 ± 40
030203-5	Charcoal	−25.7	860 ± 40
030203-9	Charcoal	−25.6	280 ± 40
BF57A	Wood	−27.5	>36,390
BF57E	Wood	−28.1	7,970 ± 70

[a]All sample preparation and analyses were done by Beta Analytic Inc. Samples BF57A and BF57E were analyzed by standard radiometric dating methods; the other samples were analyzed using accelerator mass spectrometry.

the southwest. *Zhou et al.* [2007] concluded that the last earthquake on this section of the Beichuan fault occurred sometime after 11,770 ± 360 yr BP, the youngest ^{14}C age derived from their trench. While their trench was flooded and partially filled in when we visited in 2003, we managed to extract two wood fragments for ^{14}C analysis, one from within the lowermost exposed prefaulting layer and one that postdates the last movement on the fault strands in the trench. The lower sample yielded a measured radiocarbon age of >36,430 yr BP, while the upper sample yielded a conventional radiocarbon age of 7970 ± 70 yr BP (Table 2). These samples appear to constrain the age of the last earthquake along this section of the Beichuan fault to sometime between 8 and 12 ka.

4.1.3. Donglingsi

[23] Three kilometers northeast of the trench site in the work of *Zhou et al.* [2007], the Beichuan fault cuts a large fluvial terrace at the village of Donglingsi (388495/3461461, Figure 5). The terrace consists of a strath cut on granitic bedrock that lies ∼15 m above the local riverbed, capped by ∼25 m of gravelly fill. The Beichuan fault forms a low scarp trending 047 across the southeastern margin of the terrace surface. The scarp is northwest-facing and is approximately 0.9 ± 0.1 m high (Figure 7).

[24] We collected amalgamated samples of granitic cobbles from the terrace fill for ^{10}Be analysis. Samples from depths of 0.6 ± 0.1 m and 1.5 ± 0.1 m below the terrace surface yielded coherent ^{10}Be results (Table 1) and are consistent with an inheritance-corrected depositional age of 12.2 ± 3.9 kyr. Given this, the minimum apparent throw rate on the Beichuan fault at this location is 0.07 ± 0.02 mm yr^{-1}. In contrast to sites closer to Baishuihe (Figure 5), here the scarp is northwest-facing. Note also that, if this age for the terrace surface is correct, it indicates incision of ∼25 m of fill and ∼15 m of bedrock since 12 ka, yielding a minimum bedrock incision rate in excess of 1 mm yr^{-1}.

4.1.4. Beichuan

[25] Near the town of Beichuan (448080/3521320), the Beichuan fault is clearly visible as a zone of subvertical, left-stepping fault strands (Figure 8). Dextral stream offsets of tens to hundreds of meters can be found along each fault strand. The fault is marked by a series of benches and linear scarps developed on fill terraces of unknown age, with the southeastern side consistently upthrown. This sense of vertical separation is also supported by the presence of an abandoned river valley, which begins at a hairpin bend on the Jin Jiang at the active trace of the Beichuan fault (Figure 8). The valley, which is flat floored and up to several hundred meters wide, rises from Beichuan to a gentle saddle and then drops to join a much smaller drainage basin to the south. Given the lack of a present-day river in the valley, we interpret the saddle as a wind gap and the valley as the abandoned paleochannel of the Jin Jiang. Oblique dextral displacement on the Beichuan fault, with the southeast side upthrown, appears to have allowed abandonment of the paleovalley and formation of the hairpin bend in the present Jin Jiang. At present, the Jin Jiang flows ∼10 km northeast, parallel to the Beichuan fault, before turning southwest again and crossing the fault.

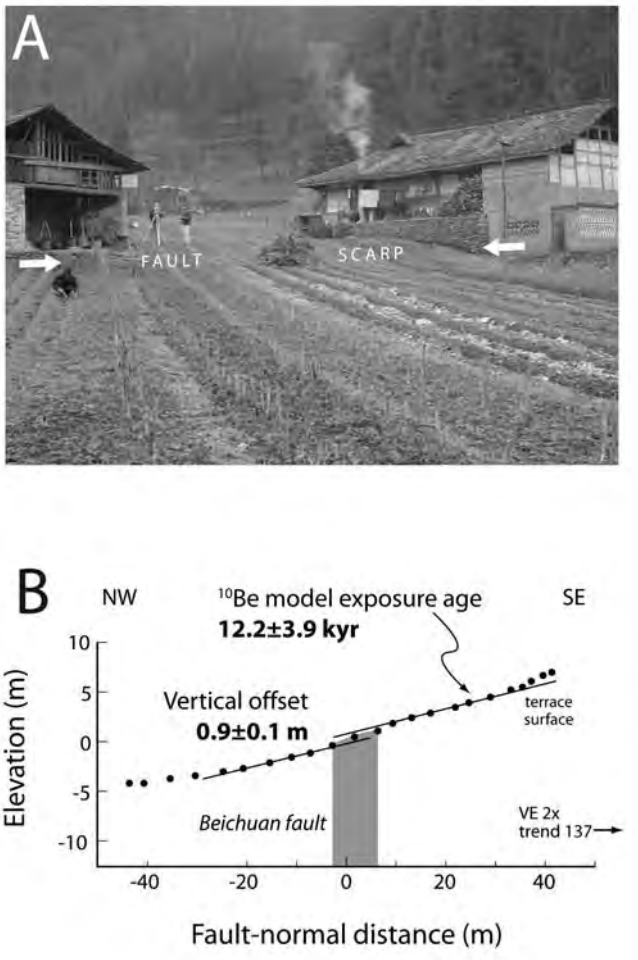

Figure 7. Scarp on fluvial fill terrace formed by the Beichuan fault at Donglingsi. See Figure 5 for location. (a) Field photo of scarp (marked by arrows) cutting terrace surface. View to the southeast. (b) Survey of scarp at the same location. The terrace surface is offset 0.9 ± 0.1 m by the fault (shown schematically by the grey box). Cosmogenic ^{10}Be samples from the terrace fill yield an inheritance-corrected age of 12.2 ± 3.9 kyr (Table 1), implying a minimum apparent throw rate of 0.07 ± 0.02 mm yr^{-1}.

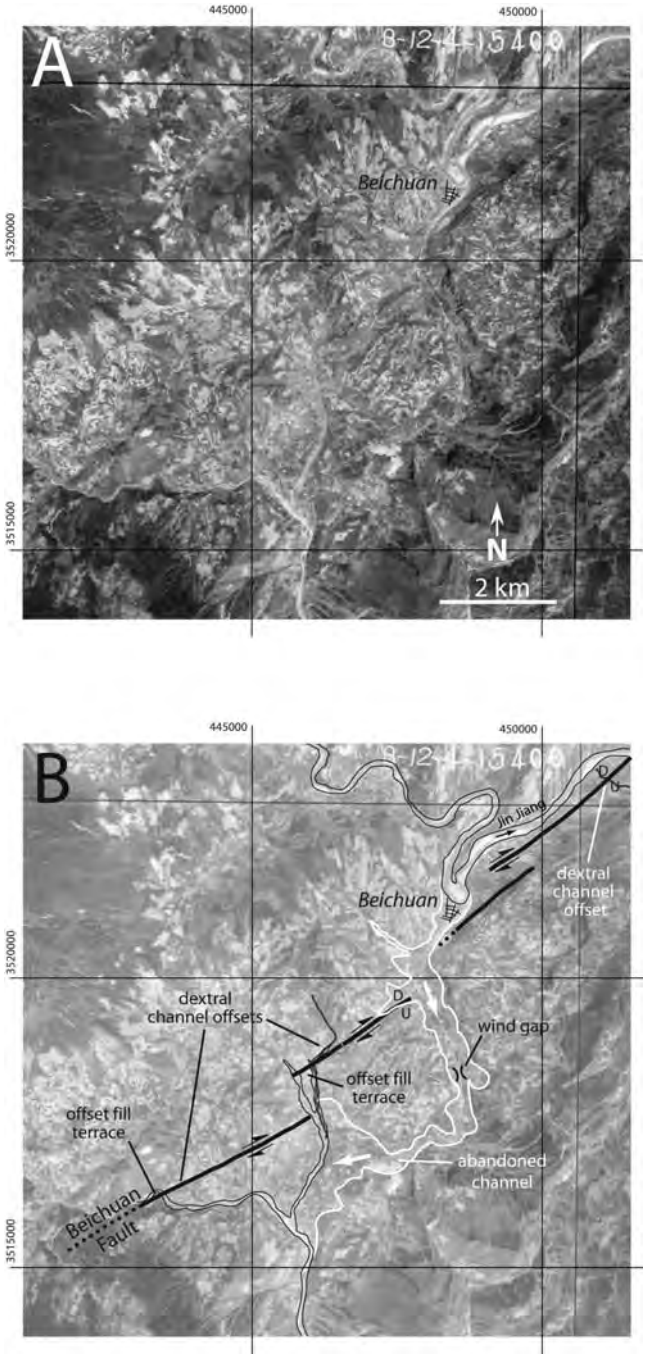

Figure 8. (a) Uninterpreted aerial photograph of the Beichuan fault near Beichuan. See Figure 1 for location. (b) Interpreted photograph of the same area. Active fault trace is marked by thick black lines. U and D mark the locally upthrown and downthrown blocks, respectively. Dark grey lines show channels which are laterally offset by the Beichuan fault. Thin white lines show margins of abandoned channel of the Jin Jiang; white arrows show inferred flow direction. The Jin Jiang is now diverted at Beichuan and flows northeast, parallel to the Beichuan fault.

4.2. Pengguan Fault

[26] Like the Beichuan fault, the Pengguan fault was active as a major crustal-scale thrust during the Late Triassic Indosinian Orogeny [*Li et al.*, 2003]. The structure that we call the Pengguan fault (Figure 1) was considered by *Chen and Wilson* [1996] to consist of two separate, colinear faults, the Xiangshui fault in the north and the Guan Xian-An Xian fault in the south. Both faults are northwest-dipping and appear to involve thrusting of pre-Indosinian rocks over syn- and post-Indosinian terrestrial sediments of the western Sichuan Foreland Basin [*Chen and Wilson*, 1996]. *Burchfiel et al.* [1995] showed a northwest-dipping thrust at the same position (for example, their Figure 9) but did not name nor describe it. Neither *Chen and Wilson* [1996] nor *Burchfiel et al.* [1995] made any mention of Quaternary slip along this structure. Our observations, primarily from the two areas described below, show that the Pengguan fault has been active in the Holocene as a dextral strike-slip fault with a small and locally variable apparent dip-slip component.

4.2.1. Shuanghe

[27] The Pengguan fault is spectacularly exposed along a linear, northeast-trending valley that extends for 15 km northeast of the town of Shuanghe (329390/3389000, Figure 9). The active trace of the fault is visible as a series of dextral stream offsets, benches, shutter ridges, linear valleys, and closed depressions along several subparallel fault strands on both sides of the valley. The Shuang He (He is also Chinese for river) has an apparent dextral offset of ~5 km; it flows southeast into the valley, turns to flow southwest along the fault, and then turns southeast again at the town of Shuanghe (Figure 9). The fault strands show both northwest-up and southeast-up senses of vertical separation; this lack of a consistent sense of dip-slip separation across the fault strands leads us to conclude that movement here is dominantly strike-slip in character. The fault appears to dextrally offset the edge of a cobble bar that sits above the confluence of the Shuang He and the Xi He (333272/3393382, Figure 9), but the offset is partially obscured by cultivation and we were unable to recover any datable material from the bar or adjacent fill terrace remnants.

[28] At Qinshiping (332065/3391701), a prominent shutter ridge forms an uphill-facing (southeast-facing) scarp, trending 048 and 2–10 m high, which offsets several streams and has led to local ponding of sediment upstream of the fault. A small stream at the northeastern end of the shutter ridge is offset by 27 ± 2 m (Figure 10). To understand the recent history of faulting at this site, we excavated a 7 × 1 × 1.5 m trench across the fault near the southwestern end of the shutter ridge (Figure 11). The trench exposed six distinct sedimentary units (Table 3) (mostly sands and clays deposited behind the shutter ridge) of which three could be traced across the fault. We found evidence for two discrete faulting events on two separate groups of structures. The first is marked by three faults (F1–F3) that cut colluvium and the basal part of a widespread sandy clay unit (unit 3 on Figure 11); these faults are in line with the prominent topographic scarp at the surface. The second event is marked by two separate faults (F4–F5), 3.5 m to the southeast, that cut the sandy-clay unit 3 but are

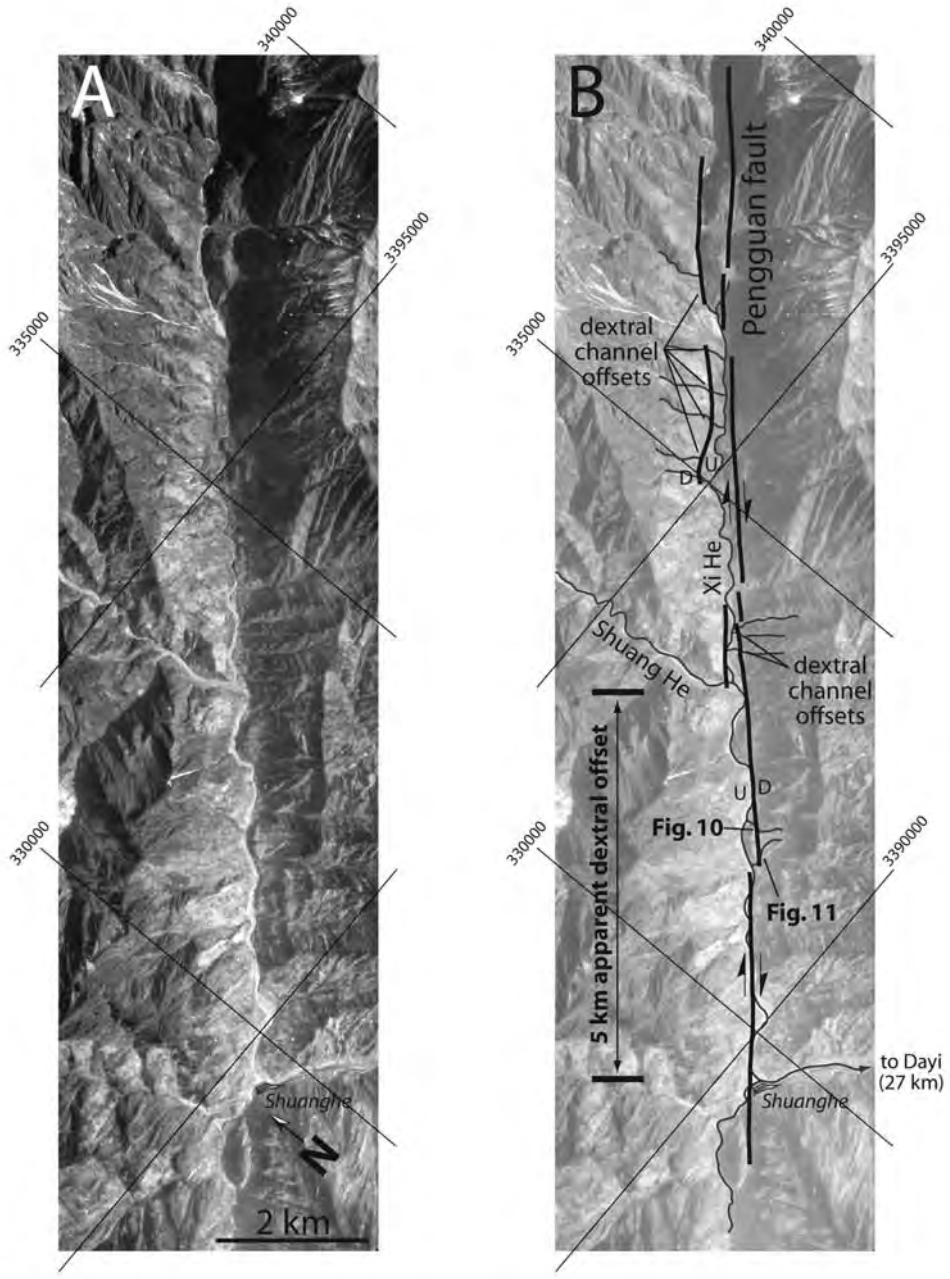

Figure 9. (a) Uninterpreted aerial photograph of the Pengguan fault near Shuanghe. See Figure 1 for location. (b) Interpreted photograph of the same area. Active fault trace is marked by thick black lines. U and D mark the locally upthrown and downthrown blocks, respectively. Dark grey lines show channels which are laterally offset by the Pengguan fault. Also shown are locations of surveyed dextral channel offset (Figure 10) and trench (Figure 11).

sealed by a distinctive upper layer that is rich in anthropogenic debris (bricks, tiles, and charcoal; unit 5 on Figure 11). Three ^{14}C ages constrain the timing of the first event to sometime before 930 ± 40 yr BP and that of the second event to between 930 ± 40 and 860 ± 40 yr BP (conventional radiocarbon years) (Figure 11 and Table 2). Displacement in both events involved minor (10–30 cm) dip slip, with the east side downthrown. We cannot constrain the magnitude, if any, of strike-slip displacement in these events, but the local geomorphology of the site and the Shuang He valley as a whole suggests that recent slip is likely to be dominantly dextral. Thus, it appears that the Pengguan fault has been active within the last thousand years at this site.

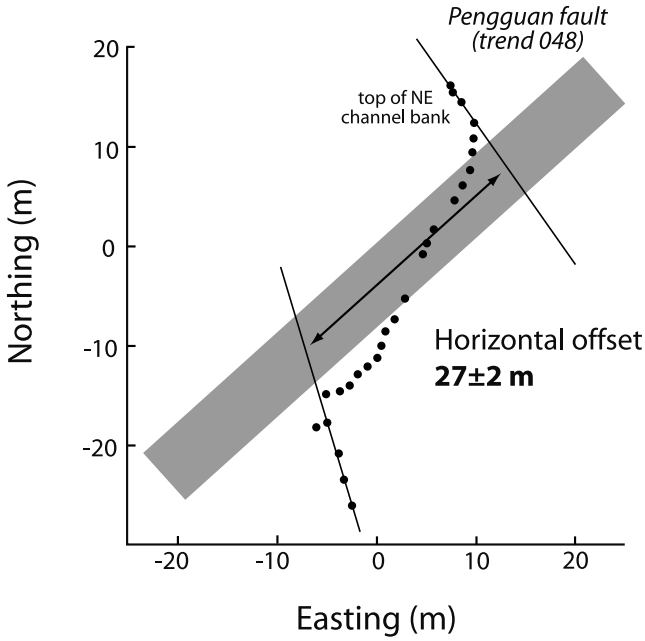

Figure 10. Map view of small channel offset by the Pengguan fault at Qinshiping. See Figure 9 for location. Black dots show survey points along the top of the northeastern channel bank, which is dextrally offset 27 ± 2 m.

4.2.2. Yongan

[29] We also examined the Pengguan fault near the village of Yongan (446829/3504427, Figure 12) in the northeastern Longmen Shan. Here the Pengguan fault bounds the southeastern margin of the broad valley of the Xi He. The active trace of the fault is visible as a linear, southeast-facing scarp trending 072 that cuts across the floodplain and low fill terraces of the Xi He (Figure 12). Near Yongan, the scarp cuts a fill terrace of the Xi He and forms a 15° right bend over a distance of about 200 m. This bend is associated with an elongate sag pond and a local increase in scarp height. Given this geometry, we interpret the sag pond as a small pull-apart basin associated with dextral strike-slip movement through the bend.

[30] At the eastern end of the sag pond, we measured a vertical scarp height of 2.6 ± 0.2 m (Figure 13). To determine the terrace depositional age, we collected a depth profile of three amalgamated subsamples of granitic and quartzite clasts for ^{10}Be analysis (Figure 14). Subsamples were collected from depths of 0.3 ± 0.05, 1.7 ± 0.1, and 3.0 ± 0.1 m below the terrace surface, which sits about 4 m above the modern river bed. Linear regression on ^{10}Be concentration as a function of depth (expressed as $\exp[-z/z_*]$) of the three subsamples, ignoring decay, yields an inheritance-corrected depositional age of 4.2 kyr, with a significant component of inherited ^{10}Be (Figure 14 and Table 1). The error on the measured ^{10}Be concentrations is relatively high, as the abundance of extractable quartz in the samples and the concentration of ^{10}Be in that quartz are both low. Given this, we conservatively estimate a model age error of ±50%. While the percent error is high, the absolute error in age (±2100 yr) is small given the goals of this study. When combined with the scarp height, the corrected depositional age is consistent with a minimum apparent throw rate of 0.62 ± 0.31 mm yr^{-1} on the Pengguan fault at this location.

4.3. Deformation Along the Longmen Shan Mountain Front

[31] Recognition of active faulting in the western Sichuan Basin is more difficult than within the plateau because of population density and intensive agriculture. Nevertheless, we have observed evidence for late Cenozoic deformation at a number of localities along the margin of the basin. While we generally lack good constraints on the timing of deformation, our observations complement and extend those described by *Burchfiel et al.* [1995].

[32] Late Cenozoic deformation along the western basin margin near the town of Dayi (358000/3385100, Figure 15) is most often expressed as a localized zone (generally ~1–2 km wide) of steeply dipping cobble to boulder conglomerate along the mountain front (Figure 16). While the mapped extent of Neogene rocks, including the cobble conglomerate of the Dayi Formation, is very limited [e.g., *Burchfiel et al.*, 1995], our observations suggest that, in fact, up to several hundred meters of conglomerate is exposed at numerous locations along the mountain front between Dujiangyan and Yaan and on the eastern and western flanks of the Xiong Po anticline (Figure 1). Where we have observed it, the conglomerate is generally steeply southeast-dipping (up to 78°) and appears to be subparallel to both (1) the unconformity that defines the base of the conglomerate and (2) bedding in the underlying sandstone and siltstone, which range from Eocene Mingshan Formation to Cretaceous Guankou Formation. Particularly good exposures of this relationship can be found at Mingshan (320061/3338449), Jindong (350543/3382169), and Jiezi (361477/3410162) (Figure 1). Dips in both the conglomerate and the underlying sedimentary rocks decrease to near zero within 1–2 km to the northwest. This localized zone of deformation along the mountain front is probably correlative with the Southeastern Marginal Fault, a blind thrust described by *Chen and Wilson* [1996]. The lack of a well-developed angular unconformity between the conglomerate and the underlying rocks suggests that surface deformation postdates (Neogene?) conglomerate deposition.

[33] Localized deformation along the mountain front is spectacularly exposed near Baitahu reservoir (365138/3393735), ~10 km northeast of Dayi (Figure 15). Excavation of a cemetery has exposed an ~200-m section through cobble conglomerate and the underlying Cretaceous Guankou Formation, just west of the mountain front (Figure 16). Bedding in the conglomerate rotates from 003/21E at the western end of the exposure to 001/46E at the center and 018/78E near the eastern end at the mountain front. The conglomerate is pervasively deformed, with numerous meter-scale faults that show dextral strike-slip and thrust kinematics. At the mountain front, we observed several

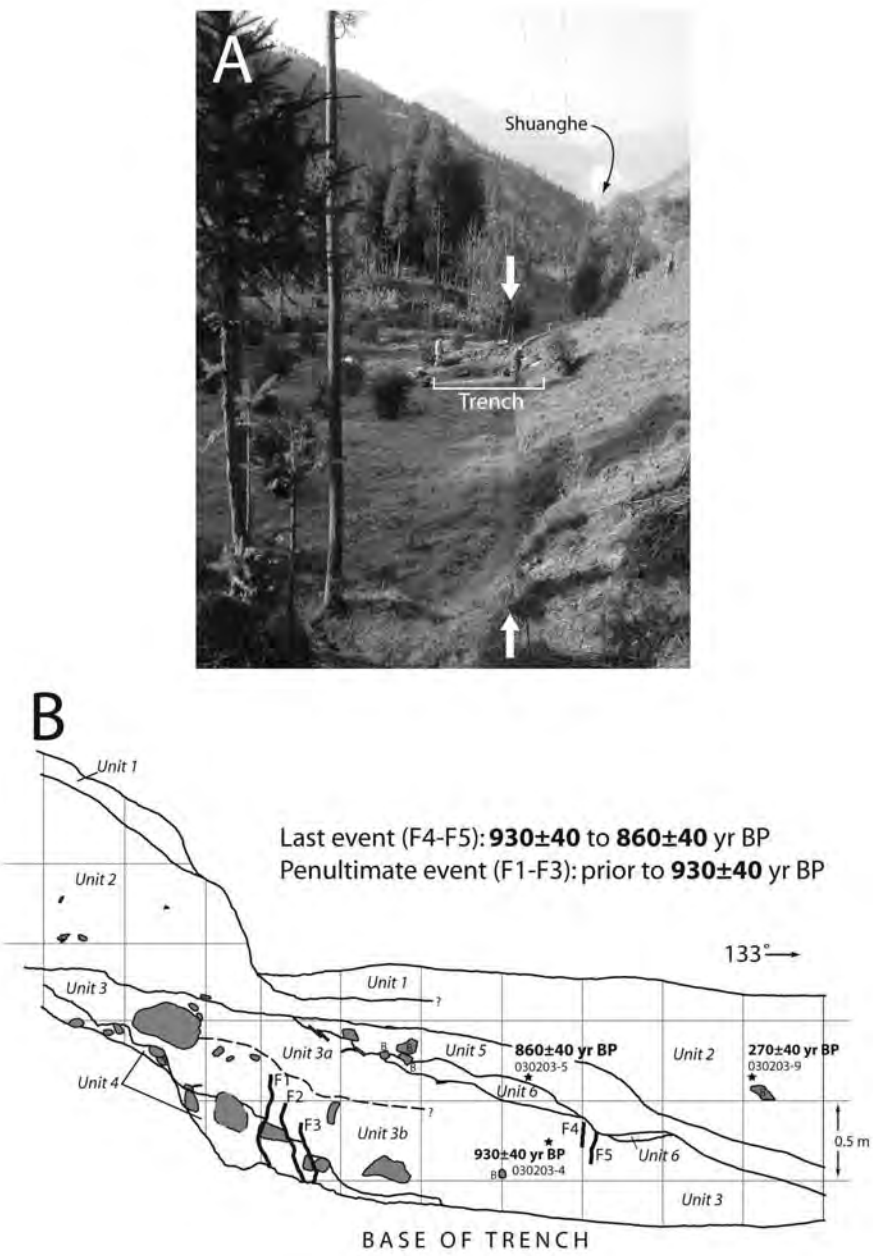

Figure 11. Trench site on the Pengguan fault at Qinshiping. See Figure 9 for location. (a) Field photo of trench site, looking southwest along the active trace of the Pengguan fault (marked by arrows). Note the east-facing scarp on the right side of photo and the shallow depression on the left. Shuanghe is visible as the plume of smoke in the background. Figures for scale. (b) Log of northeastern trench wall. Grid is 0.5 m. Black lines separate units 1–6. See Table 3 for description of units. Dark grey objects are individual cobble or boulder clasts. B, bricks. Faults F1–F5 shown by heavy black lines. Stars show locations of ^{14}C samples (Table 2). Conventional radiocarbon ages are shown in bold type. Two separate faulting events are recorded in the trench.

elongate, subparallel, *en echelon* folds that trend 030 (oblique to the mountain front, which trends 036) and fold unconsolidated red clayey sand and pebble conglomerate. Because of their elongate shape and oblique trend to the mountain front, we interpret these folds as pressure ridges associated with dextral strike-slip along a surface-rupturing fault at the front, known to Chinese geologists as the Dayi fault. The presence of a surface-rupturing fault at Baitahu is supported by a series of dextral stream offsets along the mountain front between Baitahu and Dayi (Figure 15).

Table 3. Lithologic Units in Qinshiping Trench, Pengguan Fault[a]

Unit	Description
1	Sandy CLAY, medium brown to grey-brown. Abundant modern plant material (roots, stems). Severely disturbed by cultivation
2	Massive slightly sandy SILT, olive grey. Rare (to 10 cm) clasts of sandstone, shale, brick. Some carbon (centimeter size). Slightly mottled dark grey in places
3	Massive sandy CLAY, medium yellow-brown. Rare clasts of angular fragments of shale and dark red-grey decomposed sandstone, <5 cm (most <1 cm), concentrated near base of unit. Sand is medium to coarse subrounded quartz. Very little carbon
3a	As unit 3, except clasts are less abundant and color is light to medium yellow-brown
3b	As unit 3, except clasts are less abundant. Contact between 3a and 3b is very faint and difficult to trace. Unit 3b is cut by faults F1–F3, while unit 3a is not
4	Clayey fine to medium SAND, medium brown to grey to reddish grey. Composed mostly of clasts (to 10 cm, but most <1 cm) of medium to dark grey-red decomposed sandstone, also some shale and limestone. Interpreted as colluvium derived from underlying conglomerate
5	Massive CLAY, olive grey to dark grey. Abundant brick, tile, and pottery fragments, charcoal, and (rare) dark grey sandstone clasts
6	Massive sandy CLAY, yellow to very light yellow-brown. No clasts. Sand is fine to medium grained quartz. Only locally developed at base of unit 5 and is distinctly lighter in color than underlying unit

[a]See Figure 9 for location.

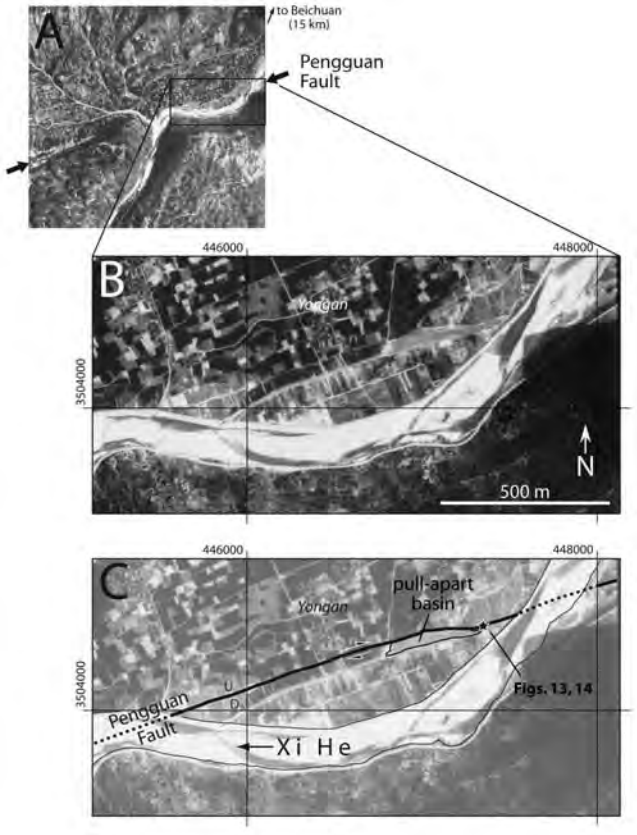

Figure 12. (a) Aerial photograph of the Pengguan fault and Xi He near Yongan. See Figure 1 for location. (b) Uninterpreted aerial photograph of the area around Yongan. (c) Interpreted photograph showing detailed view of fault where it cuts floodplain and low terrace of the Xi He. Active fault trace is marked by thick black lines. U and D mark the locally upthrown and downthrown blocks, respectively. Note small basin associated with right step in fault trace, forming a shallow lake. Location of cosmogenic sample XH-1 shown by star.

Offsets range up to several tens of meters in magnitude (for example, at 364608/3392238, Figure 17).

5. Discussion

[34] Taken in aggregate, our observations of active faulting in the Longmen Shan region share two important characteristics. First, evidence for Quaternary dextral strike-slip is ubiquitous on northeast-trending faults in both the plateau margin and at the western edge of the Sichuan Basin. The zone of Quaternary dextral slip is broader still if we include the Wenchuan-Maowen fault, as argued by *Burchfiel et al.* [1995]. These observations are in broad agreement with the model of distributed dextral shear between eastern Tibet and south China proposed by *England and Molnar* [1990]. Second, Quaternary vertical separation along the faults examined here is generally small (on the order of a few meters), and its sense varies between different places and different fault strands over length scales as short as

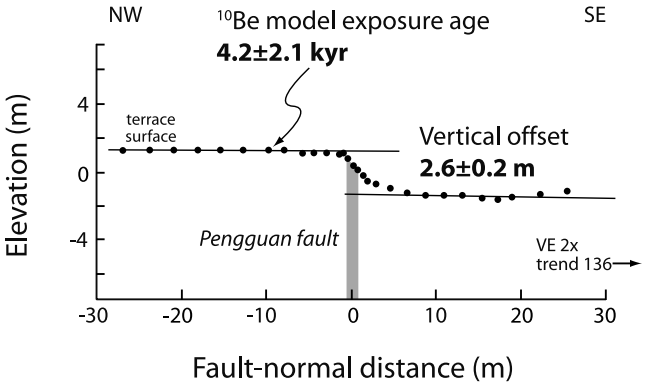

Figure 13. Survey of fluvial fill terrace cut by the Pengguan fault near Yongan. See Figure 12 for location. The fan surface is offset 2.6 ± 0.2 m across the fault (shown schematically by the grey box). Cosmogenic ^{10}Be samples from the terrace fill yield an inheritance-corrected age of 4.2 ± 2.1 kyr (Table 1 and Figure 14), implying a minimum apparent throw rate of 0.62 ± 0.31 mm y^{-1}.

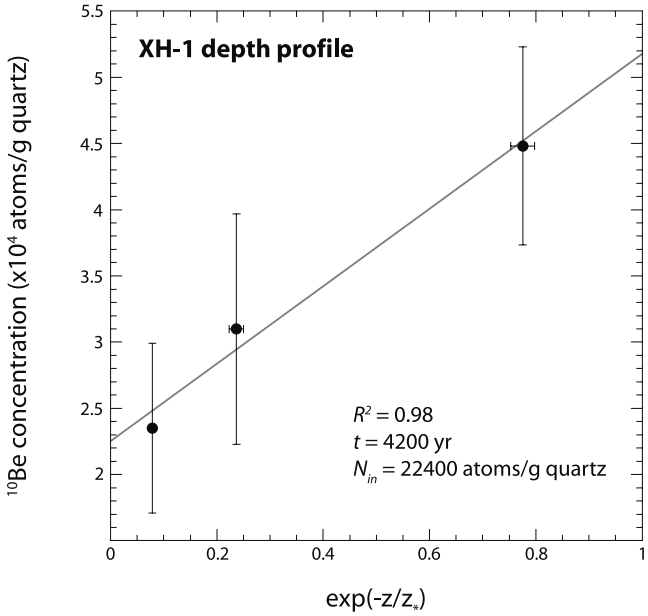

Figure 14. Depth profile of ^{10}Be subsamples from the XH-1 sample site near Yongan. See Figure 12 for location. Linear regression of $\exp(-z/z_*)$ against ^{10}Be concentration yields a model age of 4.2 kyr, with a significant component of inherited ^{10}Be (N_{in}). Model age error is conservatively estimated at ±50% or ±2.1 kyr.

a few kilometers. This variability would appear to rule out significant oblique (dextral-thrust) Quaternary displacement. The Wenchuan-Maowen, Beichuan, and Pengguan faults were all active in the Late Triassic as large-magnitude, northwest-dipping thrusts, with transport directions toward the southeast [*Chen and Wilson*, 1996]. In contrast, Quaternary activity along these faults has clearly been predominantly strike-slip, and the simplest interpretation of these fault kinematics and the linearity of the active fault traces is that the active faults are subvertical to vertical structures which may crosscut the older thrusts at depth. Given the complex network of faults in the Longmen Shan region (Figure 2) [*Burchfiel et al.*, 1995; *Chen and Wilson*, 1996; *Ma*, 2002], it is not clear how Quaternary deformation is taken up at the ends of the structures that we have identified or how deformation is distributed in the complex region between the northeast-striking dextral faults of the Longmen Shan and the large northwest-striking faults of the Xianshuihe system (Figure 1) [*Wang et al.*, 1998; *Wang and Burchfiel*, 2000].

[35] Quaternary slip rates on the dextral faults in the Longmen Shan remain largely unknown. Our ^{10}Be data provide direct evidence only for the apparent dip-slip component of the displacement rates, which is variable and ranges from 0.1 to 0.7 mm yr^{-1}. Given the widespread and compelling geomorphological evidence for a dextral strike-slip to dip-slip ratio of at least 5–10 (and possibly more), late Quaternary strike-slip rates are likely to be at least several times greater. Active strike-slip deformation is also permitted by recent GPS studies in the region [*Zhang et al.*, 2004], which suggest up to several millimeters per year of active slip across the margin. *Meade* [2007] estimated fault kinematics and slip rates by inverting GPS surface velocities from the GPS data of *Zhang et al.* [2004]; in his model, the Longmen Shan mountain front is characterized by aggregate dextral slip of ~3 mm yr^{-1} and convergence of ~2 mm yr^{-1}, broadly consistent with our geomorphic observations. GPS-derived rates of fault slip, however, are well known to be inconsistent with those derived or inferred from geological data, both in the India-Tibet collision region [e.g., *Wallace et al.*, 2004] and elsewhere [*Dixon et al.*, 2003; *Oskin and Iriondo*, 2004]. The relative dearth of seismicity in the Longmen Shan region [*Chen et al.*, 1994], coupled to our observations of latest Quaternary surface ruptures, suggest that the accumulation of strain may be more complicated than a simple linear increase over time, which is the necessary assumption in requiring GPS-derived and geologically derived rates of deformation to match.

[36] The distributed nature of active dextral strike-slip in the Longmen Shan region, and the lack of consistent

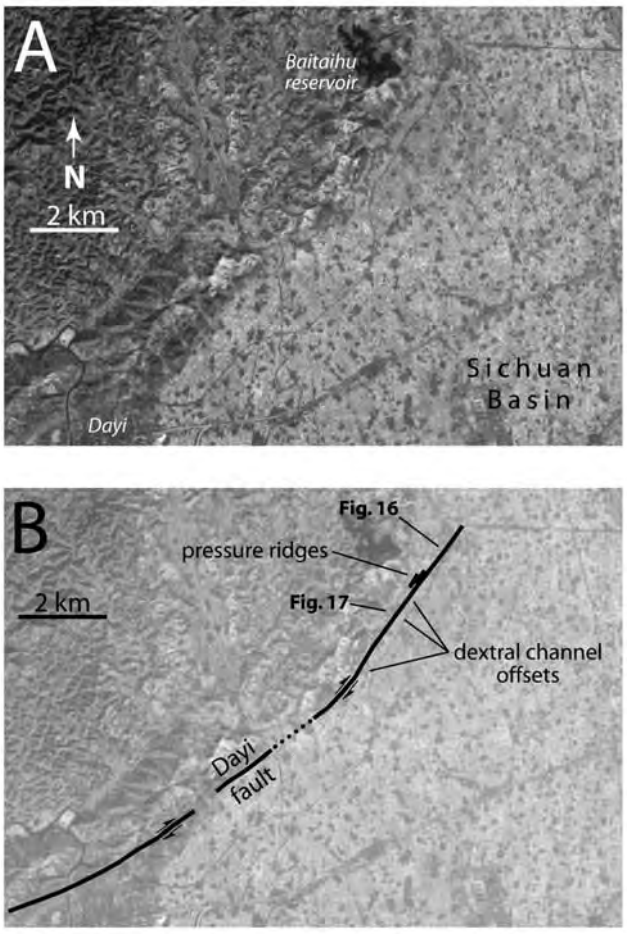

Figure 15. (a) Uninterpreted aerial photograph of the Dayi fault near Dayi. See Figure 1 for location. (b) Interpreted photograph of the same area. Active fault trace is marked by thick black lines. Pressure ridges and small-scale channel offsets near Baitahu reservoir yield dextral sense of offset.

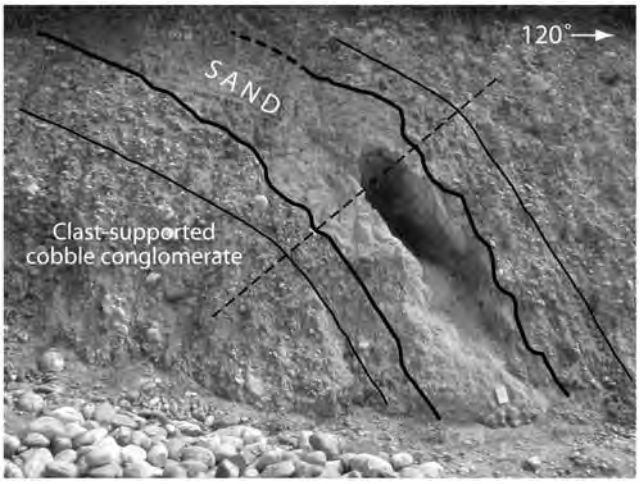

Figure 16. Field photo of steeply dipping, clast-supported cobble conglomerate of the Dayi Formation near Baitahu, 10 km northeast of Dayi. See Figure 15 for location. View is to the northeast. Clasts are dominantly subrounded-rounded cobbles of granitic rocks, with minor limestone and sandstone. Matrix is reddish-tan silty sand. Crude bedding defined by sand bed and aligned conglomerate clasts defines an open monocline (hinge shown by dashed line). Active trace of Dayi fault is ~200 m to the southeast (to the right).

differential vertical movement, provide further evidence that the present-day topographic relief between the Tibetan Plateau and the Sichuan Basin is not due to late Cenozoic slip on upper crustal faults [e.g., *Burchfiel et al.*, 1995; *Royden et al.*, 1997]. *Kirby et al.* [2003] used river profile analysis to argue against focused, differential rock uplift on faults along the margin, noting instead that river steepness (used as a proxy for rock uplift rate) appears to increase over a broad zone ~50 km adjacent to the margin. The lack of direct geomorphic evidence for Quaternary crustal shortening lends credence to this argument. It seems clear that some alternative mechanism of base level change must be invoked to explain the high present relief of the plateau margin.

[37] The margin-parallel faults do, however, appear to be important in controlling the location of large northeast-trending river valleys, and in this sense, they contribute to the local (i.e., valley floor to ridge crest) relief in the Longmen Shan (Figure 1). Local relief of 3–4 km is common on the Min Jiang where it flows along the Wenchuan-Maowen fault, along the Jian Jiang where it flows along the Beichuan fault, and on the Shuang He where it flows along the Pengguan fault (Figure 1). The margin-parallel faults act as conduits along which rapid erosion can occur, driven by relative base level change between the Tibetan Plateau and the Sichuan Basin [*Richardson et al.*, 2007]. In this sense, the present-day drainage system of the Longmen Shan region bears a striking resemblance to that of the Swiss Alps, in which the two largest rivers (the Rhine and Rhone) flow through deep, orogen-parallel valleys, localized along old thrust faults, before turning across strike to debouch into the foreland [*Schlunegger et al.*, 2001]. The spatial coincidence of the margin-parallel faults, high valley relief, and large amounts of Cenozoic denudation (up to 7–10 km; *Xu and Kamp* [2000]) suggests, but does not demand, a causal link, with the possibility that faulting and concomitant weakening of the upper crust has focused erosion along the margin-parallel valleys, promoting rock uplift of the plateau margin.

[38] Finally, our observations of fault activity in the late Pleistocene and Holocene have important implications for seismic hazard, particularly in the densely populated Sichuan Basin. We have shown evidence for surface-rupturing earthquakes along the Beichuan fault since 12–13 ka, along the northern Pengguan fault since about 4 ka, and along the southern Pengguan fault since 930 ± 40 yr BP. The timing of the last earthquake along the Dayi fault and associated structures at the mountain front is unknown, but these faults show some evidence for late Quaternary slip. An additional seismic hazard, not discussed here, is the possibility of coseismic rupture on blind or partially blind faults underlying the active Xiong Po and Longquan anticlines in the western Sichuan Basin (Figure 1) [e.g., *Burchfiel et al.*, 1995]. With the exception of the 1933 Diexi earthquake [*Chen et al.*, 1994] and the 1976 Songpan earthquake series [*Jones et al.*, 1984], the Longmen Shan region has had little historical seismicity [*Chen et al.*, 1994]. This study shows that this quiescence may not be representative of the longer timescales (~10^4 yr) relevant to geomorphology.

6. Conclusions

[39] We have documented Quaternary activity on a set of large northeast-striking faults that parallel the eastern margin of the Tibetan Plateau, using a combination of field

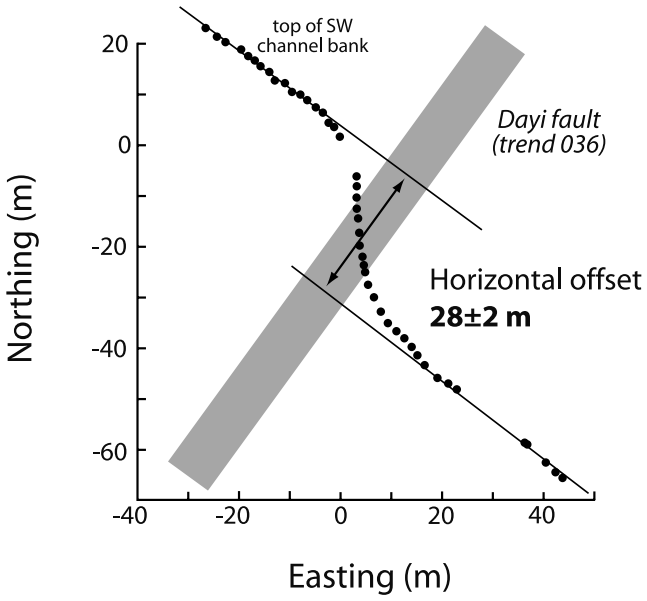

Figure 17. Map view of small channel offset by the Dayi fault near Baitahu. See Figure 15 for location. Black dots show survey points along the top of the southwestern channel bank, which is dextrally offset 28 ± 2 m.

observations, photo and image interpretation, and ^{10}Be exposure dating of offset depositional landforms. The northeast-trending Beichuan, Pengguan, and Dayi faults, which parallel the eastern margin of the Tibetan Plateau, have been active in the latest Quaternary with a dominantly dextral sense of slip. Apparent throw rates are highly spatially variable but are typically <1 mm yr^{-1}. Compelling and widespread geomorphic evidence for dominant dextral strike-slip displacement suggests to us that total displacement rates may be at least several millimeters per year. The Beichuan and Pengguan faults have experienced surface rupture during the latest Pleistocene and at some locations during the Holocene. The faults are sufficiently long to sustain a strong ground-shaking earthquake, making them potentially serious sources of regional seismic hazard.

[40] **Acknowledgments.** This research was supported by US National Science Foundation grant EAR-0125565, ETH Forschungskommission grant TH-4/03-01, and China National Natural Science Foundation grant 49802013. This is CERI contribution 512. We are very grateful to the faculty, staff, and drivers of the Chengdu University of Technology for their support. We thank Melissa Swartz, Li Bing, Si Guanying, Wang Mo, and Zhang Yi for their assistance in the field, and Philip Allen, Diane Seward, and Chris Wilson for useful discussions. Two anonymous reviewers and the Tectonics associate editor provided useful comments which significantly improved the clarity and presentation of the results. Eric Kirby, George Hilley, and Manfred Strecker provided valuable comments on an earlier version of this manuscript. Finally, we thank the people of the Longmen Shan region for their unending curiosity, hospitality, and generosity.

References

Anderson, R. S., J. L. Repka, and G. S. Dick (1996), Explicit treatment of inheritance in dating depositional surfaces using in situ ^{10}Be and ^{26}Al, *Geology*, *24*, 47–51.

Arne, D., B. Worley, C. Wilson, S. Chen, D. Foster, Z. Luo, S. Liu, and P. H. G. M. Dirks (1997), Differential exhumation in response to episodic thrusting along the eastern margin of the Tibetan Plateau, *Tectonophysics*, *280*, 239–256.

Avouac, J. P., and P. Tapponnier (1993), Kinematic model of active deformation in central Asia, *Geophys. Res. Lett.*, *20*, 895–898.

Brown, E. T., E. J. Brook, G. M. Raisbeck, F. Yiou, and M. D. Kurz (1992), Effective attenuation lengths of cosmic rays producing ^{10}Be and ^{26}Al in quartz: Implications for exposure age dating, *Geophys. Res. Lett.*, *19*, 369–372.

Burchfiel, B. C., Z. Chen, Y. Liu, and L. H. Royden (1995), Tectonics of the Longmen Shan and adjacent regions, *Int. Geol. Rev.*, *37*, 661–735.

Chen, S., and C. J. L. Wilson (1996), Emplacement of the Longmen Shan Thrust-Nappe Belt along the eastern margin of the Tibetan Plateau, *J. Struct. Geol.*, *18*, 413–430.

Chen, S., C. J. L. Wilson, and B. A. Worley (1995), Tectonic transition from the Songpan-Garze fold belt to the Sichuan Basin, southwestern China, *Basin Res.*, *7*, 235–253.

Chen, S., C. J. L. Wilson, Q. Deng, X. Zhao, and Z. Luo (1994), Active faulting and block movement associated with large earthquakes in the Min Shan and Longmen Mountains, northeastern Tibetan Plateau, *J. Geophys. Res.*, *99*, 24,025–24,038.

Chengdu Hydrological and Engineering Team (1979), *Quaternary Geologic Map of the Chengdu Plain*, Sichuan Geological Bureau, Chengdu, China.

Chengdu Hydrological and Engineering Team (1985), *Hydrology and Engineering Geology Survey of the Chengdu Plain*, Sichuan Geological Bureau, Chengdu, China.

Clark, M. K., and L. H. Royden (2000), Topographic ooze: Building the eastern margin of Tibet by lower crustal flow, *Geology*, *28*, 703–706.

Clark, M. K., L. H. Royden, K. X. Whipple, B. C. Burchfiel, X. Zhang, and W. Tang (2006), Use of a regional, relict landscape to measure vertical deformation of the eastern Tibetan Plateau, *J. Geophys. Res.*, *111*, F03002, doi:10.1029/2005JF000294.

Clark, M. K., M. A. House, L. H. Royden, K. X. Whipple, B. C. Burchfiel, X. Zhang, and W. Tang (2005), Late Cenozoic uplift of southeastern Tibet, *Geology*, *33*, 525–528.

Deng, Q., S. Chen, and X. Zhao (1994), Tectonics, seismicity, and dynamics of the Longmen Shan Mountains and its adjacent regions, *Seismol. Geol.*, *16*, 389–403.

Dixon, T. H., E. Norabuena, and L. Hotaling (2003), Paleoseismology and Global Positioning System: Earthquake-cycle effects and geodetic versus geologic fault slip rates in the Eastern California shear zone, *Geology*, *31*, 55–58.

England, P., and P. Molnar (1990), Right-lateral shear and rotation as the explanation for strike-slip faulting in eastern Tibet, *Nature*, *344*, 140–142.

Hancock, G. S., R. S. Anderson, O. A. Chadwick, and R. C. Finkel (1999), Dating fluvial terraces with ^{10}Be and ^{26}Al profiles: Application to the Wind River, Wyoming, *Geomorphology*, *27*, 41–60.

Ji, X., X. Tao, and J. Peng (1997), China Geological Survey Report, Huojing Sheet.

Jiang, F., and X. Wu (1999), The age of the Xigeda Formation, Luding, Sichuan Province, and tectonic significance, *Acta Geol. Sin.*, *73*, 1–5.

Jones, L. M., W. B. Han, E. Hauksson, A. S. Jin, Y. G. Zhang, and Z. Luo (1984), Focal mechanisms and aftershock locations of the Songpan earthquakes of August 1976 in Sichuan, China, *J. Geophys. Res.*, *89*, 7697–7707.

Kirby, E., K. X. Whipple, W. Tang, and Z. Chen (2003), Distribution of active rock uplift along the eastern margin of the Tibetan Plateau: Inferences from bedrock channel longitudinal profiles, *J. Geophys. Res.*, *108*(B4), 2217, doi:10.1029/2001JB000861.

Kirby, E., K. X. Whipple, B. C. Burchfiel, W. Tang, G. Berger, Z. Sun, and Z. Chen (2000), Neotectonics of the Min Shan, China: Implications for mechanisms driving Quaternary deformation along the eastern margin of the Tibetan Plateau, *Bull. Geol. Soc. Am.*, *112*, 375–393.

Kirby, E., P. W. Reiners, M. A. Krol, K. X. Whipple, K. V. Hodges, K. A. Farley, W. Tang, and Z. Chen (2002), Late Cenozoic evolution of the eastern margin of the Tibetan Plateau: Inferences from ^{40}Ar/^{39}Ar and (U-Th)/He thermochronology, *Tectonics*, *21*(1), 1001, doi:10.1029/2000TC001246.

Kohl, C. P., and K. Nishiizumi (1992), Chemical isolation of quartz for measurement of in-situ-produced cosmogenic nuclides, *Geochim. Cosmochim. Acta*, *56*, 3583–3587.

Lebedev, S., and G. Nolet (2003), Upper mantle beneath Southeast Asia from S velocity tomography, *J. Geophys. Res.*, *108*(B1), 2048, doi:10.1029/2000JB000073.

Li, Y., P. A. Allen, A. L. Densmore, and X. Qiang (2003), Evolution of the Longmen Shan Foreland Basin (western Sichuan, China) during the Late Triassic Indosinian Orogeny, *Basin Res.*, *15*, 117–138.

Ma, L. (2002), *Geological Atlas of China*, 348 pp., Geological Publishing House, Beijing.

McCalpin, J. P. (1996), Field techniques in paleoseismology: Introduction, in *Paleoseismology*, edited by J. P. McCalpin, pp. 33–83, Elsevier, New York.

Meade, B. J. (2007), Present-day kinematics at the India-Asia collision zone, *Geology*, *35*, 81–84.

Oskin, M., and A. Iriondo (2004), Large-magnitude transient strain accumulation on the Blackwater fault, Eastern California shear zone, *Geology*, *32*, 313–316.

Richardson, N., A. L. Densmore, D. Seward, and Y. Li (2005), Extreme exhumation within the Sichuan Basin: Late Cenozoic erosion, sedimentation, and tectonics at the eastern margin of the Tibetan Plateau based on apatite fission track thermochronology, *Eos Trans AGU*, *86*, Fall Meet. Suppl., Abstract T41A-1279.

Richardson, N., A. L. Densmore, D. Seward, A. Fowler, M. Wipf, M. A. Ellis, Y. Li, and Y. Zhang (2007), Extraordinary denudation in the Sichuan Basin: Insights from low-temperature thermochronology adjacent to the eastern margin of the Tibetan Plateau, *J. Geophys. Res.*, doi:10.1029/2006JB004739, in press.

Royden, L. H., B. C. Burchfiel, R. W. King, E. Wang, Z. Chen, F. Shen, and Y. Liu (1997), Surface deformation and lower crustal flow in eastern Tibet, *Science*, *276*, 788–790.

Schlunegger, F., J. Melzer, and G. Tucker (2001), Climate, exposed source rock lithologies, crustal uplift and surface erosion: A theoretical analysis calibrated with data from the Alps/North Alpine Foreland Basin system, *Int. J. Earth Sci.*, *90*, 484–499.

Stone, J. O. (2000), Air pressure and cosmogenic isotope production, *J. Geophys. Res.*, *105*, 23,753–23,759.

Wallace, K., G. Yin, and R. Bilham (2004), Inescapable slow slip on the Altyn Tagh fault, *Geophys. Res. Lett.*, *31*, L09613, doi:10.1029/2004GL019724.

Wang, E., and B. C. Burchfiel (2000), Late Cenozoic to Holocene deformation in southwestern Sichuan and adjacent Yunnan, China, and its role in formation of the southeastern part of the Tibetan Plateau, *Bull. Geol. Soc. Am.*, *112*, 413–423.

Wang, E., B. C. Burchfiel, L. H. Royden, L. Chen, J. Chen, W. Li, and Z. Chen (1998), Late Cenozoic Xianshuihi-Xiaojiang, Red River, and Dali fault systems of southwestern Sichuan and central Yunnan, China, *Geol. Soc. Am. Spec. Paper 327*, 108 pp.

Weislogel, A. L., S. A. Graham, E. Z. Chang, J. L. Wooden, G. E. Gehrels, and H. Yang (2006), Detrital zircon provenance of the Late Triassic Songpan-Ganzi complex: Sedimentary record of collision of the North and South China blocks, *Geology*, *34*, 97–100.

Xu, G., and P. J. J. Kamp (2000), Tectonics and denudation adjacent to the Xianshuihe fault, eastern Tibetan Plateau: Constraints from fission-track thermochronology, *J. Geophys. Res.*, *105*, 19,231–19,251.

Yin, A., and S. Nie (1996), A Phanerozoic palinspastic reconstruction of China and its neighboring regions,

in *The Tectonic Evolution of Asia*, edited by A. Yin and M. Harrison, pp. 442–485, Cambridge Univ. Press, New York.

Zhang, P. Z., et al. (2004), Continuous deformation of the Tibetan Plateau from global positioning system data, *Geology*, *32*, 809–812.

Zhou, D., and S. A. Graham (1996), Songpan-Ganzi Triassic flysch complex of the West Qinling Shan as a remnant ocean basin, in *The Tectonic Evolution of Asia*, edited by A. Yin and M. Harrison, pp. 281–299, Cambridge Univ. Press, New York.

Zhou, R., Y. Li, A. L. Densmore, M. A. Ellis, Y. He, F. Wang, and X. Li (2007), Active tectonics of the eastern margin of the Tibetan Plateau, in *The Geology of the Eastern Margin of the Tibetan Plateau*, edited by Y. Li, Geological Publishing House, Beijing, in press.

A. L. Densmore, Institute of Hazard and Risk Research and Department of Geography, Durham University, Durham, DH1 3LE, UK. (a.l.densmore@durham.ac.uk)

M. A. Ellis, Center for Earthquake Research and Information, University of Memphis, Memphis, TN 38152, USA.

G. S. Hancock, Department of Geology, College of William and Mary, Williamsburg, VA 23187, USA.

Y. Li, National Key Laboratory of Oil and Gas Reservoir Geology and Exploitation, Chengdu University of Technology, Chengdu 610059, Sichuan, China.

N. Richardson, Department of Earth Sciences, Swiss Federal Institute of Technology, CH-8092 Zurich, Switzerland.

R. Zhou, Seismological Bureau of Sichuan Province, Chengdu 610041, Sichuan, China.